

RESEARCH ON CHAOTIC FEATURES OF A FLOW FIELD OVER A PLUNGING AIRFOIL BASED ON DYNAMIC MODE DECOMPOSITION

YUHANG QI

School of Aeronautics, Northwestern Polytechnical University, Xi'an, China

WENQING YANG

*School of Aeronautics, Northwestern Polytechnical University, Xi'an, China, and
Research and Development Institute of Northwestern Polytechnical University in Shenzhen, Shenzhen, China
e-mail: yangwenqing@nwpu.edu.cn*

YUE WANG

School of Aeronautics, Northwestern Polytechnical University, Xi'an, China

BIFENG SONG

*School of Aeronautics, Northwestern Polytechnical University, Xi'an, China, and
Yangtze River Delta Research Institute of Northwestern Polytechnical University, Taicang, China*

Periodic motion of a plunging airfoil causes continuous changes in the surrounding flow field. The time-dependent thrust coefficient depends entirely on unsteady characteristics of the flow field. On the contrary, the time-dependent thrust coefficient may also reflect the unsteady characteristics of the corresponding flow field. With the fast Fourier transform (FFT) and dynamic mode decomposition (DMD), unsteady aerodynamic forces can be correlated with the flow field characteristics in the frequency domain. In the present paper, DMD is performed to analyze the unsteady characteristics of the flow field around a plunging NACA0012 airfoil at the Reynolds number of 20 000.

Keywords: plunging airfoil, chaotic flow, dynamic mode decomposition, thrust characteristic, irregularity

1. Introduction

Flapping-wing aerodynamics has attracted many researchers' interest in the recent decades due to its unique unsteady characteristics. The fact that the oscillating airfoil produces thrust was first discovered in (Knoller, 1909; Betz, 1912) and then verified by experiments (Katzmayr, 1922). The flow characteristics of a plunging airfoil are analyzed and the corresponding wakes are classified into three categories: drag-producing wake, neutral wake and thrust-producing wake (Jones *et al.*, 1998), respectively. When the airfoil is in non-sinusoidal plunging motions (Srikumar *et al.*, 2018), the effects of motions on the thrust performance are investigated under various unsteady parameters. The velocity profiles in the wake of a plunging airfoil were discussed in (Davari, 2017).

The transition of a flow over an oscillating airfoil from periodicity to chaos has aroused widespread research interest. When the reduced frequency and Strouhal number are low, periodic and asymmetric wakes can be clearly observed. As the reduced frequency and Strouhal number increase, some asymmetric and aperiodic phenomena may appear in the wake of a two-dimensional (2D) heaving airfoil (Lewin and Haj-Hariri, 2003). And it is found that the wake pattern depends primarily on the evolution of the leading-edge vortex. By increasing the oscillation amplitude, a chaotic flow is observed (Blondeaux *et al.*, 2005). It should be noted that the

quasi-periodic regime exhibits transient unstable characteristics and may also result in chaotic dynamics. Visbal (2009) found through numerical simulation that the chaotic flow generated in 2D cases did not exist in three-dimensional (3D) cases. The argument that asymmetric wake was suppressed by the 3D effects was experimentally supported by Calderon *et al.* (2014), because the tip vortex created in 3D cases could prevent vortex coupling. Interacting vortices can cause the thrust coefficients to be different in two different plunging cycles (Ashraf *et al.*, 2012). When the plunging amplitude is large, the flow will transit from periodicity to quasi-periodicity, or even chaos at last. The result shows that the chaotic flow is not an artifact of the 2D flow field assumption. In 3D cases, the leading-edge vortices are stable and coherent when the plunging frequency is low but the plunging amplitude is large, and they begin to break down into small vortex structures when the plunging frequency becomes higher and the plunging amplitude becomes smaller. Therefore, in the 2D flow field behind the NACA0012 airfoil undergoing a coupled pitching and plunging motion, the vortex interaction plays an important role in chaotic transition and the chaotic wake (Bose and Sarkar, 2018). As the plunging amplitude gradually increases, the flow field undergoes transition from periodicity to chaos through a quasi-periodic route. The leading-edge flow separation may give a rise to an aperiodic wake. Several fundamental vortex interaction mechanisms take place in the periodic or quasi-periodic flow. And these interactions become completely erratic in the chaotic flow. At a higher reduced frequency and a larger plunging amplitude, the flow of the airfoil undergoing non-sinusoidal plunging motion was found to be aperiodic by Srikumar *et al.* (2018). Meanwhile, many different tools are also used to study chaotic features by analyzing the time-dependent lift and thrust coefficients, such as Fourier spectra and phase maps (Khalid *et al.*, 2018).

Dynamic mode decomposition (DMD) was first proposed by Schmid and Sesterhenn (2008) on an academic conference, which provide a convenient tool for extracting flow information to describe flow characteristics (Schmid *et al.*, 2009). DMD is a pure data-driven algorithm that does not require governing equations (Taira *et al.*, 2017), which has been used to extract dynamic information from flow field generated by numerical simulation or measured by physical experiments (Schmid, 2010).

Development of the DMD method based on model reduction algorithms, such as the optimized DMD (Chen *et al.*, 2012) and sparsity-promoting DMD (Jovanović *et al.*, 2014) has also raised considerable concern. A great deal of research has been done to improve the computational efficiency. For example, a fast method to perform DMD in real time on large data sets (Hemati *et al.*, 2014), a method to perform DMD in parallel (Belson *et al.*, 2014), and a tensor-based DMD method requiring fewer memory resources have been successively proposed (Klus *et al.*, 2018). And the recursive dynamic mode decomposition method was presented by Noack *et al.* (2016).

Chen *et al.* (2012) concluded that the data should be neither periodic nor from a linear process for DMD to construct a meaningful modal decomposition. Therefore, DMD is suitable for analyzing chaotic flows. The performance of DMD was investigated by Noack *et al.* in an aperiodic flow behind three rotating cylinders (Noack *et al.*, 2016). As the flow is aperiodic, the amplitudes and spatial patterns of DMD modes extracted from a one-cycle flow field are quite different from those from a two-cycle flow field at the same temporal frequencies (Yu *et al.*, 2018). The aperiodic flow results in incomplete flow information from a single oscillation cycle. More dynamically important DMD modes can be extracted from the three-cycle flow information. More energetic DMD modes with lower frequencies can be extracted when more flow information is available. Based on these results, DMD can be used to investigate chaotic flows over a plunging airfoil.

The present work aims at examining the effects of the plunging amplitude on the flow field at a given reduced frequency and Reynolds number. The DMD method is used to analyze the flow transition from periodicity to chaos through a quasi-periodic route as the plunging

amplitude gradually increases. The study cases are described and verified in Section 2.1, and DMD methodology is explicated in Section 2.2. The results of modal analysis from one-cycle information are discussed in Section 3.1, the aperiodic behaviors are analyzed in Section 3.2, and the effects of the plunging amplitude on stability are examined in Section 3.3 with conclusions being drawn in Section 4.

2. Study cases and methodology

A NACA0012 airfoil with chord length of $c = 0.1$ m is selected for numerical simulation, where the Reynolds number Re is 20 000, the flow is set to water, and U_∞ is 0.201 m/s.

2.1. Numerical schemes

The unsteady flow field around the plunging airfoil is numerically simulated by the commercial computational fluid dynamics package Fluent. Ashraf *et al.* (2012) proved that the results of NS laminar equations and the Spalart-Allmaras turbulent model are identical and in good agreement with the experimental data. Therefore, the viscous flow is set as laminar. The second-order scheme is used for spatial discretization, and the transient formula is set as second-order implicit. Results are obtained on a structured O-mesh with the first cell height of 0.02 mm to ensure that y^+ is less than 1.0. The computational mesh size is 299×101 (airfoil surface \times normal airfoil) as shown in Fig. 1.

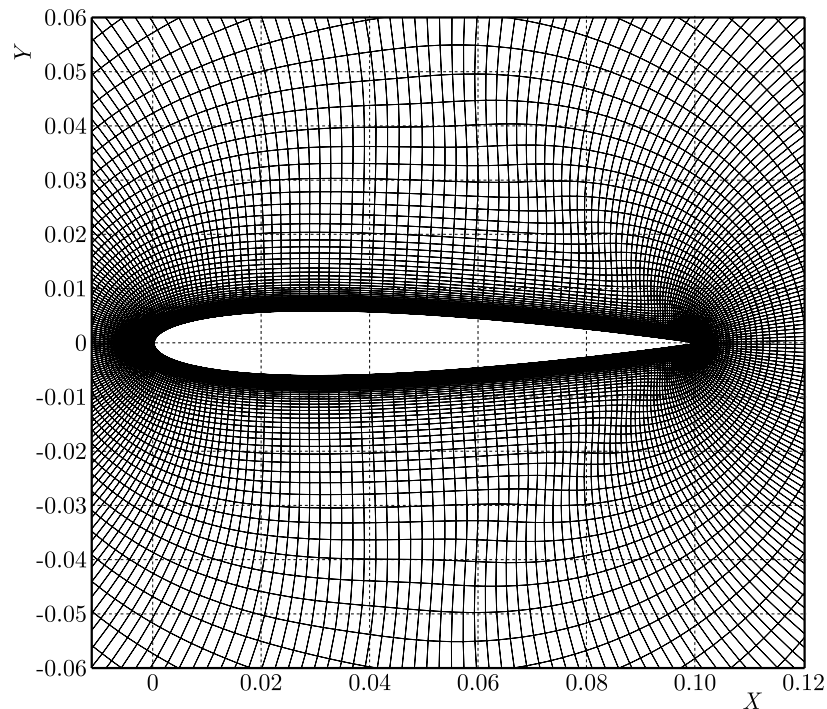


Fig. 1. Mesh around the airfoil

The sinusoidal plunging motion of the airfoil is specified as follows

$$y = h_0 \sin(2\pi ft) \quad (2.1)$$

where y is the position of the plunging airfoil, h_0 is the plunging amplitude and f is the plunging frequency. The reduced frequency $k = 2\pi fc/U_\infty$ is set to a fixed value of 1.0, and $f = 0.3199$.

The mesh independence study is carried out at a nondimensional plunging amplitude of $h = h_0/c = 0.50$ with three mesh sizes: (a) 99×101 , (b) 199×101 , and (c) 299×101 . It makes no difference if points in the normal direction are doubled (Ashraf *et al.*, 2012). For each of these cases, 800 time steps are selected in a cycle. It is observed that the mesh with a size of 299×101 is sufficiently refined and the thrust coefficient is mesh independent, as shown in Fig. 2a. Based on such results, the mesh size of 299×101 is selected for the following simulation.

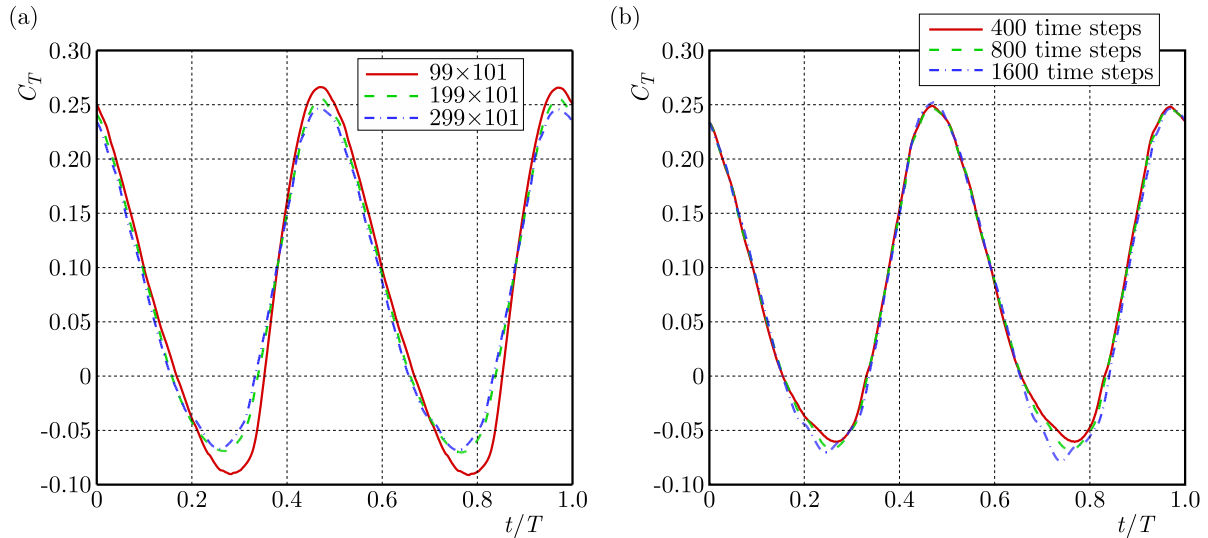


Fig. 2. Time-dependent thrust coefficient at $h = 0.50$: (a) different mesh resolutions, (b) different time steps

As shown in Fig. 2b, the simulation is carried out in which three different time steps of 400, 800 and 1600 are selected for time steps refinement. For 1600 time steps per cycle, there is a slight difference between the two minimum values of the time-dependent thrust coefficient. At the same time, the minimum value of time-dependent thrust coefficient decreases as the time steps increase from 400 to 800. Therefore, the mesh size of 299×101 and 800 time steps per cycle are adopted for all subsequent simulations in the present work.

The values of the non-dimensional plunging amplitude selected for the present work are $h = 0.25, 0.50, 1.00, 1.25, \text{ and } 1.50$. Figure 3 shows the effects of the plunging amplitude on the time-averaged thrust coefficient. In each case, 10 plunging cycles are run, and the corresponding mean value is calculated from the last 4 plunging cycles based on the research explored by Srikumar *et al.* (2018), with the results being compared to the reference ones from the numerical simulations by Ashraf *et al.* (2012) and Srikumar *et al.* (2018). In Fig. 3, 7-10T denotes the time-averaged thrust coefficient from the last 4 plunging cycles, and 9T stands for the time-averaged thrust coefficient from the 9th plunging cycle. Aperiodic behavior was discovered by Ashraf *et al.* (Ashraf *et al.*, 2012). It can be seen that the time-dependent thrust coefficient varies from one cycle to the next one when k_h is large enough resulting in a different time-averaged thrust coefficient calculated from each cycle. Therefore, the time-averaged thrust coefficient from the 9th cycle is calculated to prove the aperiodic behavior. The numerical time-averaged thrust coefficients from the last 4 plunging cycles are in good agreement with the reference values. Some discrepancy occurs between the single 9T data and the reference data, which will be explained in depth below. However, the variation trend of 9T is consistent with that of the reference data.

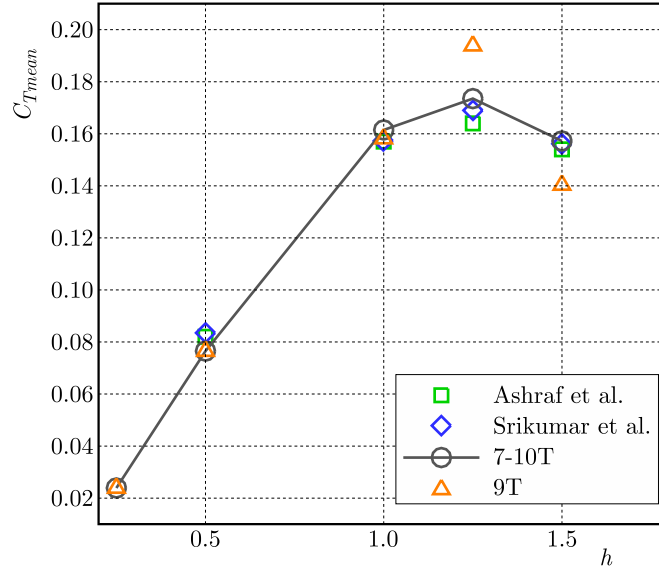


Fig. 3. Variation of C_{Tmean} with h

2.2. Dynamic mode decomposition

The DMD method introduced by Schmid *et al.* (2009) is adopted to analyze a series of “snapshots” of the flow past the airfoil. Parameters such as the sampling frequency are presented in Section 3. These snapshots v_i can be arranged in a matrix \mathbf{V}_1^N and two lagged matrices

$$\begin{aligned}\mathbf{V}_1^N &= \{v_1, v_2, v_3, \dots, v_N\} \\ \mathbf{V}_1^{N-1} &= \{v_1, v_2, v_3, \dots, v_{N-1}\} \\ \mathbf{V}_2^N &= \{v_2, v_3, \dots, v_N\}\end{aligned}\quad (2.2)$$

A linear mapping A is assumed, which propagates the flow field from a one instant time step to the next

$$v_i = Av_{i+1} \quad (2.3)$$

So the relation between \mathbf{V}_1^{N-1} and \mathbf{V}_2^N is defined as follows

$$A\mathbf{V}_1^{N-1} = \mathbf{V}_2^N \quad (2.4)$$

The last snapshot can be expressed as a linear combination of the previous ones

$$v_n = a_1v_1 + a_2v_2 + \dots + a_{N-1}v_{N-1} + r \quad (2.5)$$

where r denotes the residual. Based on Eq. (2.4), the matrices \mathbf{V}_1^{N-1} and \mathbf{V}_2^N are related as follows

$$A\mathbf{V}_1^{N-1} = \mathbf{V}_2^N = \mathbf{V}_1^{N-1}\mathbf{S} + re_{N-1}^T \quad (2.6)$$

To compute the matrix \mathbf{S} , the singular value decomposition (SVD) is to be performed

$$\text{SVD}(\mathbf{V}_1^{N-1}) = \mathbf{U}\mathbf{\Sigma}\mathbf{V}^T \quad \mathbf{V}_2^N = \mathbf{U}\mathbf{\Sigma}\mathbf{V}^T\mathbf{S} \quad (2.7)$$

Finally, the matrix $\tilde{\mathbf{S}}$, an approximation of A , is expressed by

$$\tilde{\mathbf{S}} = \mathbf{U}^T\mathbf{V}_2^N\mathbf{V}\mathbf{\Sigma}^{-1} \quad \tilde{\mathbf{S}}\mathbf{y}_i = \mu_i\mathbf{y}_i \quad \Phi_i = \mathbf{U}\mathbf{y}_i \quad (2.8)$$

where μ_i and \mathbf{y}_i represent the eigenvalue and eigenvector of $\tilde{\mathbf{S}}$, respectively, and Φ contains the DMD modes

$$\lambda = \frac{\log \mu}{\Delta t} \quad (2.9)$$

where Δt is the time interval between adjacent snapshots.

The growth/decay rates and frequencies of the DMD modes can be obtained by calculating the real and imaginary parts of λ . So the real part of λ ($\Re(\lambda)$) can be used to analyze the stability characteristics of the modes. Positive values for the real part of λ denote that the modes are growing, whereas the negative values for the real part of λ denote that the modes are decaying. The larger absolute value of $\Re(\lambda)$, the faster the spatial patterns grow or decay. For a specific mode, if the real part of λ is zero, it indicates that this mode is neutrally stable; and if the imaginary part of λ is zero, it indicates that this mode denotes the mean flow with the zero frequency. Since the eigenvalues usually appear as complex conjugate pairs, there exist conjugate modes with the same real part but the opposite imaginary part of λ . The modes with a negative imaginary part of λ are neglected herein, that is the modes discussed herein have non-negative frequencies (non-negative imaginary part).

3. Results and discussion

The analysis herein is based on the vorticity data from numerical simulations validated in Section 2.1. As the number of sampling periods increases, the results of DMD analysis become complicated. Due to aperiodic characteristics, the flow information from a single plunging cycle is incomplete, and new DMD modes can be extracted from the two-cycle flow information (Yu *et al.*, 2018). Therefore, the work herein presents the results from one cycle, two cycles and four cycles, respectively.

3.1. Connection between the thrust and modes

The phenomena resulting from a change in the plunging amplitude are analyzed with data from the 9th plunging cycle. First, the thrust coefficient varying with time at $h = 0.25$, 1.25 and 1.50 is shown in Fig. 4. At $h = 0.25$, the sinusoidal time-dependent thrust coefficient is presented. When the plunging amplitude increases from $h = 0.25$ to $h = 1.25$, the sinusoidal time-dependent thrust coefficient varies irregularly with time, and this variation becomes highly irregular at $h = 1.50$. The time-averaged thrust coefficient increases with the increasing non-dimensional plunging amplitude within a certain range, as shown in Fig. 3, and meanwhile, the time-dependent thrust coefficient curve with time becomes irregular as h increases. This is due to the effects of the plunging amplitude on flow structures. The flow and DMD modes extracted from the flow will be explained later.

The thrust coefficient from the 9th plunging cycle is selected for FFT (fast Fourier transform) analysis, and DMD analysis is performed based on the corresponding vorticity data. The frequency spectrum of the thrust coefficient and the distribution of the amplitude and $\Re(\lambda)$ with their corresponding frequency from different DMD modes are shown in Fig. 5. The spatial patterns (real parts) for modes of $k_w \approx 0, 1, 2$ are displayed in Fig. 6. $k_w = 2\pi f_t c / U_\infty = \omega c / U_\infty$ represents the frequency, f_t denotes the frequency derived by FFT, and ω is the imaginary part of λ . Based on this, the frequencies derived respectively from FFT and DMD are unified. From the spectrum of the thrust coefficient, the frequency component of $k_w = 1$ does not contribute much to the thrust coefficient due to the small amplitude at $h = 0.25$ and 1.25. However, compared with DMD modes of $k_w \approx 0$ and 2, the amplitude of the corresponding DMD mode of $k_w \approx 1$ is not small, which explains that the corresponding DMD mode of $k_w \approx 1$ is important

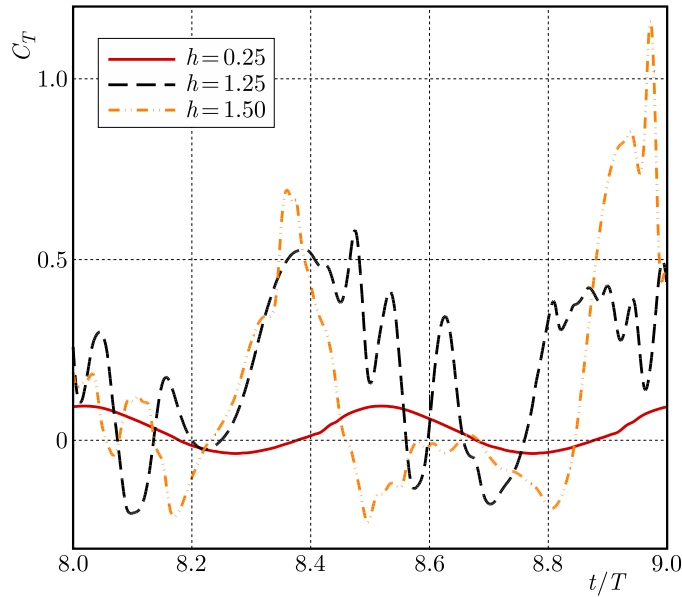


Fig. 4. Time-dependent thrust coefficient from the 9th plunging cycle at $h = 0.25, 1.25$ and 1.50

to flow structures and has no effect on the thrust coefficient. When the plunging amplitude increases to $h = 1.50$, the amplitude of the FFT component of $k_w = 1$ is equal to the mean thrust coefficient, so the DMD mode of $k_w \approx 1$ is important for producing the thrust. As shown in Fig. 6, the spatial patterns for the DMD mode of $k_w \approx 1$ are approximate at $h = 1.25$ and 1.50 , while these two modes contribute differently to the thrust. With DMD, the spatial patterns that have important influence on the thrust performance can be extracted from the corresponding flow field.

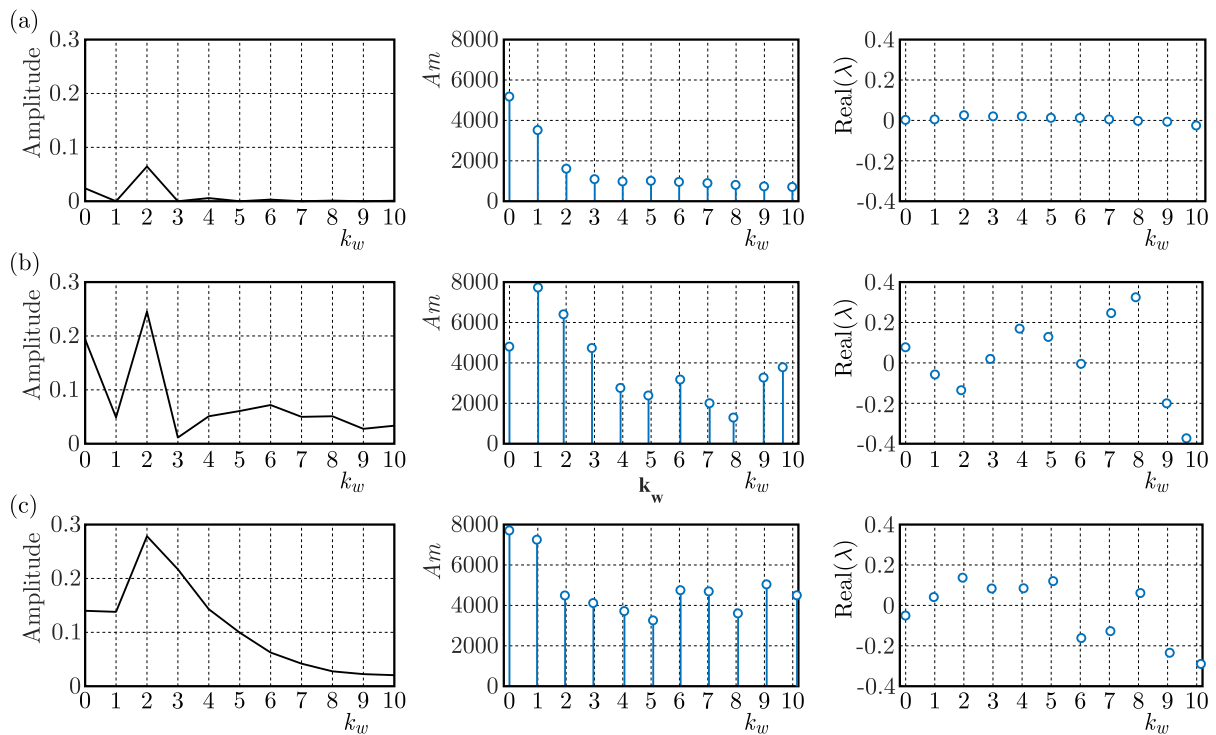


Fig. 5. FFT of the thrust coefficient (left), distribution of the amplitude (middle) and $\Re(\lambda)$ (right) of DMD modes with their corresponding frequency: (a) $h = 0.25$, (b) $h = 1.25$, (c) $h = 1.50$

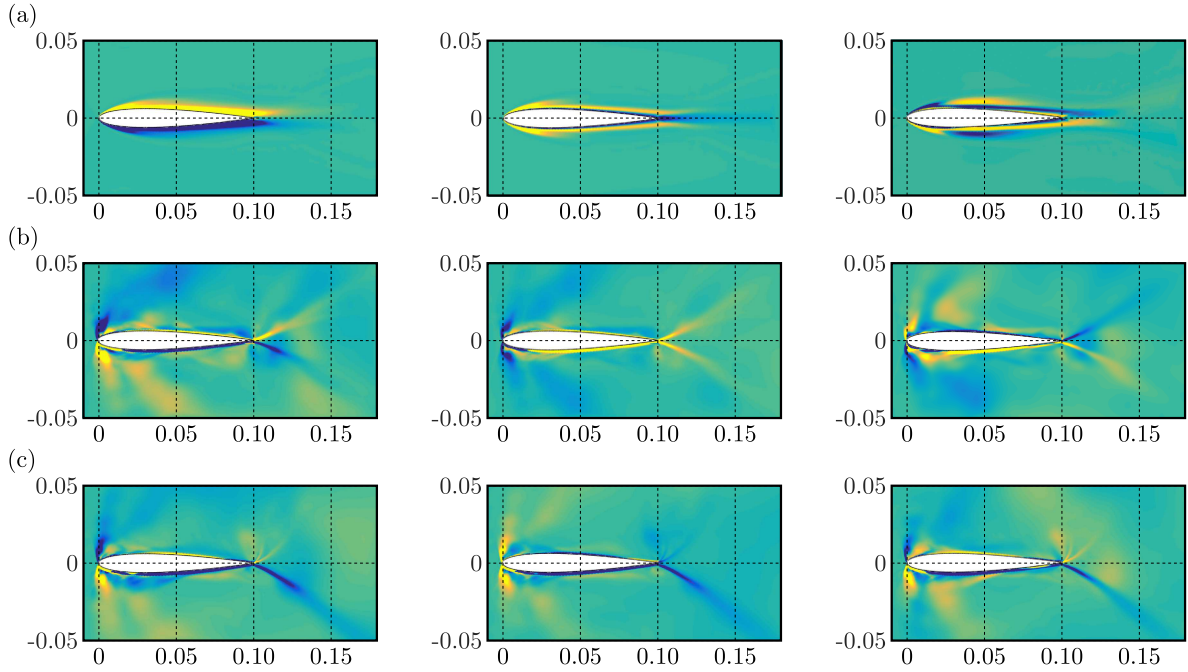


Fig. 6. Spatial patterns (real part) for DMD modes of $k_w \approx 0$ (left), 1 (middle), and 2 (right):
 (a) $h = 0.25$, (b) $h = 1.25$, (c) $h = 1.50$

As mentioned earlier, the $\Re(\lambda)$ of DMD modes provide information about the stability of the corresponding flow structure. The first 11 dominant $\Re(\lambda)$ are shown in Fig. 5. At $h = 0.25$, these DMD modes are neutrally stable; because the associated $\Re(\lambda)$ is close to the neutral line ($\Re(\lambda) = 0$). These modes are neither growing nor decaying but just kept unchanged, which explains to some extent why the corresponding thrust coefficient presents cosinusoidal features. When the plunging amplitude increases to $h = 1.25$ and 1.50 , the $\Re(\lambda)$ moves away from the neutral line. As shown in Fig. 4, since the DMD modes are either growing or decaying, the associated thrust coefficient shows a certain twist.

Several important modes ($k_w \approx 0$, 1, and 2) extracted from the vorticity field are shown in Fig. 6. DMD captures coherent structures with the same frequency (Yu *et al.*, 2018). So the disordered vortex structures are transformed into simple coherent structures. The flow structures in Fig. 6a show a long vortex region over the airfoil at $h = 0.25$. At $h = 1.25$ and 1.50 , the spatial patterns are similar and the leading-edge vortex structures and the long wake are clearly shown in Fig. 6b and 6c. But the growth/decay rates of the two similar DMD stationary modes are opposite. At $h = 1.25$, the associated DMD stationary mode is growing, while at $h = 1.50$, the stationary mode is decaying. This phenomenon provides a scope for explaining why the corresponding time-averaged thrust coefficient decreases when h increases from 1.25 to 1.50 .

3.2. Aperiodic behavior

DMD is used to analyze the chaotic flow field, where the data is selected from two different plunging cycles (9th and 10th plunging cycles). Figure 7 compares the time-dependent thrust coefficient of two plunging cycles for cases where $h = 0.50$, 1.00 , and 1.25 at $k = 1.0$. At $h = 0.50$, the time-dependent thrust coefficient is periodic. An aperiodic feature appears at $h = 1.00$, and the chaotic feature is prominent at $h = 1.25$. That is why the mean thrust coefficients of 9T and 7-10T are different at large plunge amplitudes.

Chen *et al.* (2012) found that the data used for DMD did not need to be periodic. And Noack *et al.* (2016) adopted the performance of DMD to investigate a aperiodic flow behind

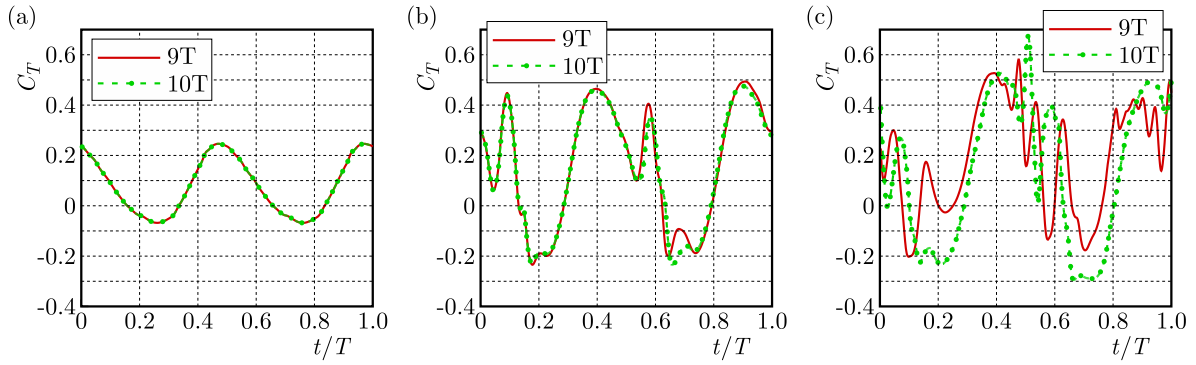


Fig. 7. Time-dependent thrust coefficient of 9T and 10T: (a) $h = 0.50$, (b) $h = 1.00$, (c) $h = 1.25$

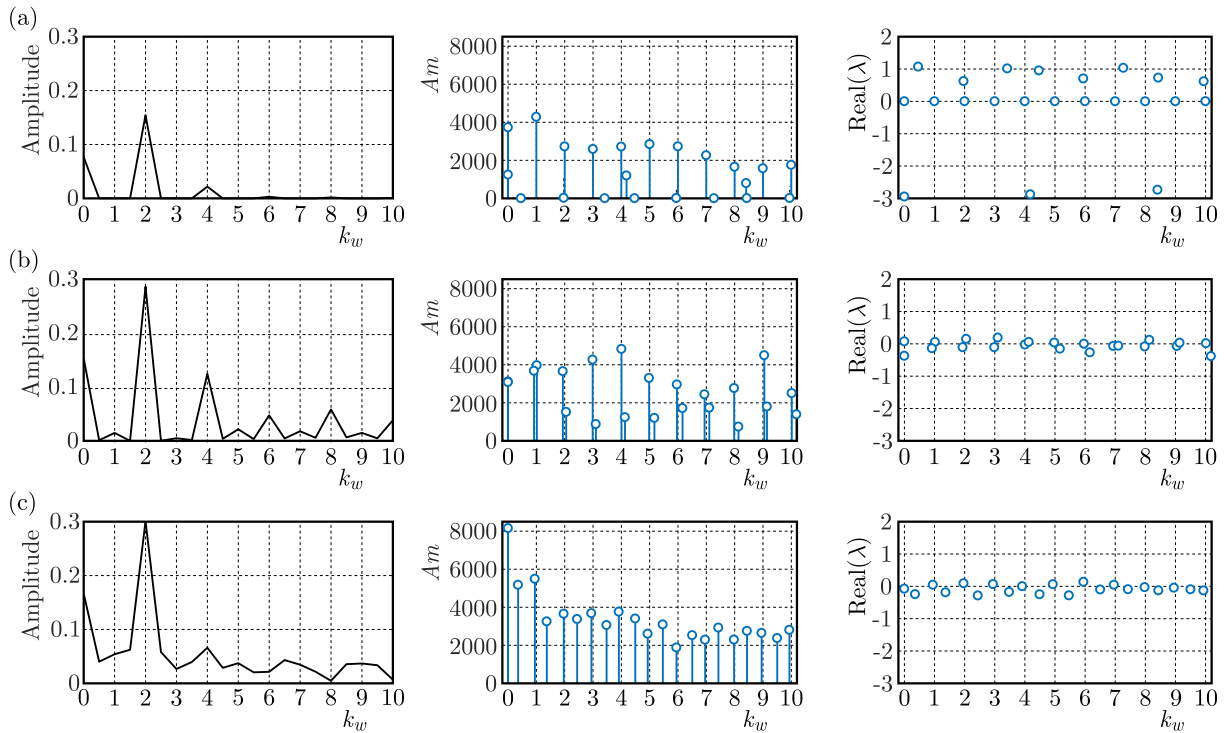


Fig. 8. FFT of the thrust coefficient (left), distribution of the amplitude (middle) and $\Re(\lambda)$ (right) of DMD modes with their corresponding frequency: (a) $h = 0.50$, (b) $h = 1.00$, (c) $h = 1.25$

three rotating cylinders. Therefore, DMD is performed to analyze the aperiodic behavior of flow fields in this Section.

The spectral content of the time-dependent thrust coefficient and DMD modes extracted from the two-cycle vorticity field data are shown in Fig. 8. For the spectral content of the time-dependent thrust coefficient, more components with a lower frequency may be extracted, and the resolution ratio may double. The minimum frequency interval decreases from 1.0 (plunging frequency) to 0.5 for k_w when the sampling time increases from one cycle to two cycles. But new findings can be observed from the distribution of DMD modes. When h is 0.50 and the flow is periodic, the new DMD modes with close frequencies (e.g., $k_w \approx 0$) or middle frequencies (e.g., $k_w \approx 0.5$) are extracted from the two-cycle flow information. These modes have either very small amplitudes or large amplitudes with large decay rates. The results show that these new DMD modes have little impact on the flow. Although the amplitudes of new DMD modes are large, the oscillating spatial patterns extracted from the flow fields decay rapidly. The influence of the corresponding spatial patterns on the flow severely weakens over time. Therefore, the dominant

DMD modes are still prominent in such a case. Since the non-dimensional plunging amplitude h is 0.5, the frequency components of $k_w \approx 0.0, 2.0$ and 4.0 greatly contribute to the thrust coefficient. With DMD, the corresponding spatial patterns that have important influence on the flow and thrust performance can be extracted from the flow field. As h increases to 1.00 and the flow becomes quasi-periodic, it is hard to identify which modes are dominant because there are two modes with a similar frequency and growth/decay rates. The frequency components of spatial patterns are close to each other, and the corresponding spatial patterns show a slow decay trend. Therefore, the new DMD modes extracted from the quasi-periodic flow are of equal importance to the flow. When h is 1.25 and the flow is chaotic, the new DMD modes with middle frequencies (e.g., $k_w \approx 0.5$ and 1.5) are extracted, such as the spectral content of the thrust coefficient, which cannot be overlooked due to its large amplitude and the low decay rate. The spatial patterns corresponding to the middle frequencies first appear as dominant flow structures.

The distribution of DMD modes may reflect the flow characteristics of the plunging airfoil. Based on DMD, the new information extracted from the periodic flow shows a weak effect on the flow. Similar information can be extracted from the quasi-aperiodic flow and new dominant information may also be extracted from the chaotic flow. More information extracted by DMD can help us to better understand the aperiodic features. The flow structures formed in the current cycle may affect the evolution of flow structures in the next cycle. Long-term vortex-vortex interactions may cause the chaotic flow when the non-dimensional plunging amplitude is large. The two-cycle flow field is analyzed by DMD. And the vortex-vortex interactions are represented by DMD modes. In the periodic flow, the interactions are weak, indicating that the new DMD modes are not dominant. However, the interactions are strong in the chaotic flow, and the extracted new DMD modes contribute substantially to the flow. These important new DMD modes can indirectly prove the existence of chaotic characteristics.

3.3. Plunging amplitude effects on stability

In the previous Section, only the DMD modes with $k_w \leq 10$ are discussed. Therefore, the stability characteristics of all DMD modes extracted from the four-cycle (starting from 7T) vorticity field data will be discussed here, except for the modes with negative frequencies. The number of growth and decay modes is shown in Table 1. It can be observed that the number of decay modes is far greater than that of the growth modes, so most of the spatial patterns extracted by DMD are in the damped oscillation state. When h increases from 0.25 to 1.00, the number of decay modes gradually increases. Therefore, the vortex structures will become more complex, but the damped oscillation will not be suppressed as h increases. When h increases from 1.00 to 1.50, the number of decay modes is stable and the number of damped oscillations spatial patterns does not vary markedly.

Table 1. Number of growth and decay modes at $h = 0.25, 0.50, 1.00, 1.25,$ and 1.50

	$h = 0.25$	$h = 0.50$	$h = 1.00$	$h = 1.25$	$h = 1.50$
$\Re(\lambda) < 0$ (decay modes)	101	108	127	119	120
$\Re(\lambda) > 0$ (growth modes)	63	55	35	41	42

The $\Re(\lambda)$ distribution of DMD modes with corresponding frequencies are shown in Fig. 9. In the figure, the range of $\Re(\lambda)$ is fixed. So the DMD modes with $\Re(\lambda) < -2$ or $\Re(\lambda) > 1$ are not shown in this figure. The corresponding solid lines with the same color are linear regression lines at each h . The corresponding linear regression lines are used to describe the $\Re(\lambda)$ distribution of DMD modes with the frequency.

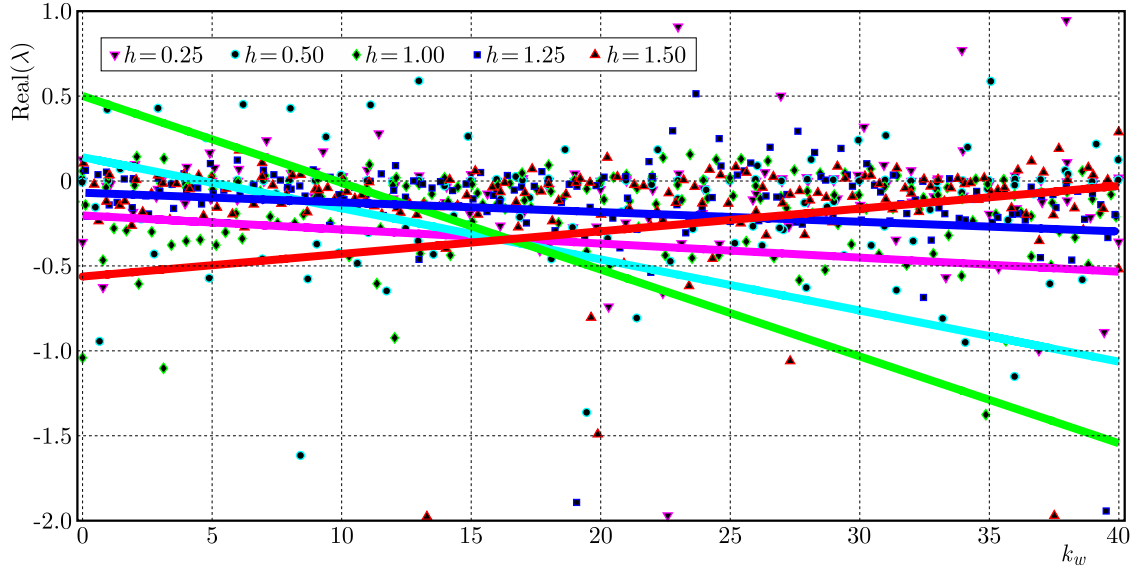


Fig. 9. Stability of all DMD modes for $h = 0.25, 0.50, 1.00, 1.25$ and 1.50 cases

The spectrum $(k_w, \Re(\lambda))$ of DMD modes seems random, but the law of variability of $\Re(\lambda)$ with the frequency is clearly shown for each case. When h is 0.25, 0.50 and 1.00, the corresponding slope of the linear regression line is negative. Therefore, the $\Re(\lambda)$ will decrease as the frequency increases. The higher the frequency, the faster the damped oscillation spatial patterns decay. When h increases from 0.25 to 1.00, the corresponding slope of the linear regression line decreases. This means that the damped oscillation spatial patterns decay faster at the same frequency when h is higher.

However, when h increases from 1.00 to 1.50, the corresponding slope of the linear regression line is increased. At $h = 1.50$, the corresponding slope of the linear regression line is positive. Therefore, the $\Re(\lambda)$ will increase as the frequency increases. At a lower frequency, the spatial patterns extracted by DMD are decaying. At a higher frequency, the spatial patterns are growing.

For the case of $h = 1.25$, the frequency has little effect on $\Re(\lambda)$, and the corresponding linear regression line is closest to the neutral line ($\Re(\lambda) = 0$). When the frequencies are lower or higher, the $\Re(\lambda)$ is close to zero. Therefore, the corresponding spatial patterns change slowly.

Meanwhile, the distribution of discrete points around the corresponding line is quantified by defining the *Error* between the discrete points and the line. The *Error* is defined as

$$Error = \sum_{i=1}^n \frac{|y_i - (ax_i + b)|}{n} \quad (3.1)$$

where at each h , a and b denote the slope and y -intercept of the linear regression line, respectively; x_i and y_i denote the frequency k_w and $\Re(\lambda)$ of DMD modes, respectively. When the value of *Error* is small, these discrete points are close to the corresponding linear regression line. When the value of *Error* is large, these discrete points are far away from the corresponding linear regression line. The corresponding results of *Error* are shown in Table 2. As h increases to 1.00, the value of *Error* is increasing and the discrete points gradually move far away from the corresponding linear regression line. At $h = 1.25$, the *Error* is minimal, and the discrete points are along the sides of the corresponding linear regression line, which is closest to the neutral line as mentioned earlier. So most points are distributed close to the neutral line. Most of the spatial patterns extracted by DMD are maintained due to their low growth/decay rates. At the same time, the mean thrust coefficient for the five cases is maximal. Therefore, it is proposed that the neutral self-stabilized flow generates the optimal thrust.

Table 2. Results of *Error* at $h = 0.25, 0.50, 1.00, 1.25$ and 1.50

	$h = 0.25$	$h = 0.50$	$h = 1.00$	$h = 1.25$	$h = 1.50$
<i>Error</i>	0.7861	0.9038	0.9237	0.2284	0.4270

4. Conclusions

DMD is used to investigate the process of flow transition from periodicity to chaos through a quasi-periodic route as the plunging amplitude gradually increases. The chaotic transition of the flow over a plunging NACA0012 airfoil is caused by the increasing plunging amplitude. The effects of the plunging amplitude on chaotic transition and stability are systematically discussed herein at a reduced frequency of 1.0 with a Reynolds number of 20 000. At the same time, the distribution of DMD modes extracted from one-cycle information and the spectral content of the corresponding thrust coefficient are presented. It is observed that the modes with frequencies of $k_w \approx 0$ and 2 have an important influence on the thrust performance. The thrust is related to the reduced modes in the frequency domain. The large growth/decay rates of DMD modes result in transition of the time-dependent thrust from smoothness to tortuosity. Periodic and aperiodic flows are distinguished by decay/growth rates extracted with DMD. When the sampled data comes from two cycles, the dominant modes extracted from the periodic flow are prominent and similar modes extracted from the quasi-periodic flow also appear. And meanwhile, new DMD modes with lower frequencies are extracted from the chaotic flow. The differences between the distribution of DMD modes extracted from periodic, quasi-periodic and chaotic flows are identified. A method to distinguish quasi-periodic and chaotic flows from flows over the plunging airfoil is provided. The last four cycles of flow data are used to analyze the flow stability by DMD. The distribution laws of the DMD spectrum are explored by the linear regression line and *Error* analysis. At a small plunging amplitude, $\Re(\lambda)$ decreases with the increasing frequency. But at a large plunging amplitude, $\Re(\lambda)$ increases with the increasing frequency. The variation trend of $\Re(\lambda)$ will change as the plunging amplitude increases. At $h = 1.25$, the $\Re(\lambda)$ is close to the neutral line, and the time-averaged thrust coefficient for five cases is the largest. It is inferred from the analysis that the neutral self-stabilized flow generates the optimal thrust performance.

Acknowledgments

This work was supported in part by the National Natural Science Foundation of China under Grant 11872314, the Key R&D Program in Shaanxi Province of China under Grant 2020GY-154 and the China Scholarship Council.

References

1. ASHRAF M.A., YOUNG J., LAI J.C.S., 2012, Oscillation frequency and amplitude effects on plunging airfoil propulsion and flow periodicity, *AIAA Journal*, **50**, 11, 2308-2324
2. BELSON B.A., TU J.H., ROWLEY C.W., 2014, Algorithm 945: modred – A parallelized model reduction library, *ACM Transactions on Mathematical Software*, **40**, 4, 30
3. BETZ A., 1912, Ein beitrage zur erklarung des segelfluges, *Zeitschrift für Flugtechnik und Motorluftschiffahrt*, **3**, 269-272
4. BLONDEAUX P., GUGLIELMINI L., TRIANTAFYLLOU M.S., 2005, Chaotic flow generated by an oscillating foil, *AIAA Journal*, **43**, 4, 918-921
5. BOSE C., SARKAR S., 2018, Investigating chaotic wake dynamics past a flapping airfoil and the role of vortex interactions behind the chaotic transition, *Physics of Fluids*, **30**, 4, 047101
6. CALDERON D.E., CLEAVER D.J., GURSUL I., WANG Z., 2014, On the absence of asymmetric wakes for periodically plunging finite wings, *Physics of Fluids*, **26**, 071907

7. CHEN K.K., TU J.H., ROWLEY C.W., 2012, Variants of dynamic mode decomposition: boundary condition, Koopman, and Fourier analyses, *Journal of Nonlinear Science*, **22**, 887-915
8. DAVARI A.R., 2017, Wake structure and similar behavior of wake profiles downstream of a plunging airfoil, *Chinese Journal of Aeronautics*, **30**, 1281-1293
9. HEMATI M.S., WILLIAMS M.O., ROWLEY C.W., 2014, Dynamic mode decomposition for large and streaming datasets, *Physics of Fluids*, **26**, 111701
10. JONES K.D., DOHRING C.M., PLATZER M.F., 1998, Experimental and computational investigation of the Knoller-Betz effect, *AIAA Journal*, **36**, 1240-1246
11. JOVANOVIĆ M.R., SCHMID P.J., NICHOLS J.W., 2014, Sparsity-promoting dynamic mode decomposition, *Physics of Fluids*, **26**, 024103
12. KATZMAYR R., 1922, Effect of periodic changes of angle of attack on behavior of airfoils, *NACA TM*, **147**
13. KHALID M.S.U., AKHTAR I., DONG H., AHSAN N., JIANG X., WU B., 2018, Bifurcations and route to chaos for flow over an oscillating airfoil, *Journal of Fluids and Structures*, **80**, 262-274
14. KLUS S., GELSS P., PEITZ S., SCHÜTTE C., 2018, Tensor-based dynamic mode decomposition, *Nonlinearity*, **31**, 3359-3380
15. KNOLLER R., 1909, Die Gesetze des Luftwiderstandes, *Flug-und Motortechnik (Wien)*, **3**, 21, 1-7
16. LEWIN G.C., HAJ-HARIRI H., 2003, Modelling thrust generation of a two-dimensional heaving airfoil in a viscous flow, *Journal of Fluid Mechanics*, **492**, 339-362
17. NOACK B.R., STANKIEWICZ W., MORZYŃSKI M., SCHMID P.J., 2016, Recursive dynamic mode decomposition of transient and post-transient wake flows, *Journal of Fluid Mechanics*, **809**, 843-872
18. SCHMID P.J., 2010, Dynamic mode decomposition of numerical and experimental data, *Journal of Fluid Mechanics*, **656**, 5-28
19. SCHMID P.J., MEYER K.E., PUST O., 2009, Dynamic mode decomposition and proper orthogonal decomposition of flow in a lid-driven cylindrical cavity, *8th International Symposium on Particle Image Velocimetry*, Melbourne, Victoria, Australia
20. SCHMID P.J., SESTERHENN J., 2008, Dynamic mode decomposition of numerical and experimental data, *61st Annual Meeting of the APS Division of Fluid Dynamics*, American Physical Soc., College Park, MD
21. SRIKUMAR G., SRIKRISHNAN V.A., PURUSHOTHAMAN R.K., THIAGARAJAN V., VELAMATI R.K., LAXMAN V., 2018, Numerical study on thrust generation in an airfoil undergoing nonsinusoidal plunging motion, *Journal of Aerospace Engineering*, **31**, 4, 04018037
22. TAIRA K., BRUNTON S.L., DAWSON S.T.M., ROWLEY C.W., COLONIUS T., MCKEON B.J., SCHMIDT O.T., GORDEYEV S., THEOFILIS V., UKEILEY L.S., 2017, Modal analysis of fluid flows: An Overview, *AIAA Journal*, **55**, 4013-4041
23. VISBAL M. R., 2009, High-fidelity simulation of transitional flows past a plunging airfoil, *AIAA Journal*, **47**, 11, 2685-2697
24. YU M., WANG B., WANG Z.J., FAROKHI S., 2018, Evolution of vortex structures over flapping foils in shear flows and its impact on aerodynamic performance, *Journal of Fluids and Structures*, **76**, 116-134